Astronomy & Astrophysics manuscript no. 1518-astroph
August 17, 2008

Multi-telescope timing of PSR J1518+4904

G. H. Janssen[1], B. W. Stappers[2,1,3], M. Kramer[3], D. J. Nice[4], A. Jessner[5], I. Cognard[6], and M. B. Purver[3]

[1] Astronomical Institute "Anton Pannekoek", University of Amsterdam, Kruislaan 403, 1098 SJ Amsterdam, The Netherlands; e-mail: gemma@science.uva.nl
[2] Stichting ASTRON, Postbus 2, 7990 AA Dwingeloo, The Netherlands; e-mail: Ben.Stappers@manchester.ac.uk
[3] University of Manchester, Jodrell Bank Observatory, Macclesfield Cheshire, SK11 9DL, UK
[4] Physics Department, Bryn Mawr College, Bryn Mawr, PA 19010, USA
[5] Max-Planck-Institut für Radioastronomie, Auf dem Hügel 69, 53121 Bonn, Germany
[6] Laboratoire de Physique et Chimie de l'Environnement, CNRS, 3A Avenue de la Recherche Scientifique, F-45071 Orléans, Cedex 2, France

Received/Accepted

ABSTRACT

Context. PSR J1518+4904 is one of only 9 known double neutron star systems. These systems are highly valuable for measuring the masses of neutron stars, measuring the effects of gravity, and testing gravitational theories.
Aims. We determine an improved timing solution for a mildly relativistic double neutron star system, combining data from multiple telescopes. We set better constraints on relativistic parameters and the separate masses of the system, and discuss the evolution of PSR J1518+4904 in the context of other double neutron star systems.
Methods. PSR J1518+4904 has been regularly observed for more than 10 years by the European Pulsar Timing Array (EPTA) network using the Westerbork, Jodrell Bank, Effelsberg and Nançay radio telescopes. The data were analysed using the updated timing software TEMPO2.
Results. We have improved the timing solution for this double neutron star system. The periastron advance has been refined and a significant detection of proper motion is presented. It is not likely that more post-Keplerian parameters, with which the individual neutron star masses and the inclination angle of the system can be determined separately, can be measured in the near future.
Conclusions. Using a combination of the high-quality data sets present in the EPTA collaboration, extended with the original GBT data, we have constrained the masses in the system to $m_p < 1.17\ M_\odot$ and $m_c > 1.55\ M_\odot$ (95.4% confidence), and the inclination angle of the orbit to be less than 47 degrees (99%). From this we derive that the pulsar in this system possibly has one of the lowest neutron star masses measured to date. From evolutionary considerations it seems likely that the companion star, despite its high mass, was formed in an electron-capture supernova.

Key words. stars: neutron – pulsars: general – pulsars: individual (PSR J1518+4904)

1. Introduction

PSR J1518+4904 was discovered in the Green Bank Northern Sky Survey (Sayer et al. 1997). It is one of only 9 double neutron star systems (DNSs) known. The pulsar orbits its companion neutron star in 8.63 days, and its 40 ms spin period, together with the derived low surface magnetic field, is typical of a mildly recycled pulsar. Nice et al. (1996) first described the system and have already shown that the space velocity is probably quite low. They also measured the periastron advance from which the total system mass was estimated. Thorsett & Chakrabarty (1999), using a Bayesian analysis with no constraints on the orientation of the orbit, found the masses of the pulsar and its companion to be $m_p = 1.56^{+0.20}_{-1.20}\ M_\odot$ and $m_c = 1.05^{+1.21}_{-0.14}\ M_\odot$ (95% confidence). An improved timing solution was presented by Hobbs et al. (2004), although not discussed in detail.

DNSs are presently the best available tool for testing strong-field gravity effects. The PSR J1518+4904 orbit is only mildly relativistic, making it of limited use for tests of gravitational theories. However, any constraints on its post-Keplerian (PK) parameters, the inclination of its orbit, or the masses of the pulsar and its companion are highly valuable for studies of the evolution of these systems (e.g. Podsiadlowski et al. 2004; Kalogera et al. 2007).

Like PSR J1811−1736 (Corongiu et al. 2007), PSR J1518+4904 has a rather wide orbit. This could indicate that the evolution into a DNS system has been slightly different than most other systems, which generally have tight orbits with periods of several hours. However, PSR J1518+4904 does follow the recently discovered spin period-eccentricity relation (Faulkner et al. 2005; Dewi et al. 2005), suggesting that the evolution cannot be too different from the tight DNSs.

PSR J1518+4904 has been observed regularly using the four 100 m class radio telescopes in Europe. This has allowed

us to select high-quality data resulting in the best possible analysis of the system parameters to date. For completeness, we have also included data from telescopes at Green Bank as presented in Nice et al. (1996, 1999). We present the new timing solution and discuss the limits our solution puts on the inclination and the masses of the neutron stars in the system. We discuss the future prospects of detecting multiple PK parameters, and we related our results to the evolution of DNSs.

2. Observations and data analysis

This research is part of the EPTA network. The extensive collection of observations from Westerbork, Jodrell Bank, Effelsberg and Nançay observatories has enabled us to select the best combinations of data sets with the best characteristics for various purposes. For example, high quality TOAs and long time spans permit better measurement of astrometric parameters, while using multiple frequencies allows us to precisely measure the dispersion measure (DM) and monitor possible DM variations. Individual properties of the data sets are presented in Table 1, and a description of the observing systems is given below.

2.1. Westerbork

PSR J1518+4904 has been observed approximately monthly since 1999 at the Westerbork Synthesis Radio Telescope (WSRT) with the Pulsar Machine (PuMa; Voûte et al. 2002), at frequencies centred at 840 and 1380 MHz, and since 2007 also occasionally at 2300 MHz. The sampling time for most observations was 102.4 μs and the bandwidth used was 8×10 MHz where each 10 MHz band was split into 64 channels. The 1380 MHz data taken after September 2006 used 80 MHz of bandwidth spread in 8 steps of 10 MHz over a range of 160 MHz. The data were dedispersed and folded off-line, and then integrated over frequency and time over the whole observation duration to get a single profile for each observation. Each profile was cross-correlated with a standard profile (Fig. 1), obtained from the summation of high signal-to-noise (S/N) profiles, to calculate a time of arrival (TOA) for each observation. These were referred to local time using time stamps from a H-maser at WSRT. The TOAs were converted to UTC using global positioning system (GPS) maser offset values measured at the observatory. For this research, we only used observations with TOA errors $< 15\,\mu s$, with an average around $8\,\mu$s.

2.2. Jodrell Bank

At Jodrell Bank, PSR J1518+4904 was observed since its discovery approximately every two weeks using the 76-m Lovell telescope. Observations were made at centre frequencies around 410, 610 and 1400 MHz. All receivers were cryogenically cooled, providing left-hand and right-hand circularly polarized signals. These signals were fed into an analogue filterbank system where the polarisations were detected, filtered, digitised at appropriate sampling intervals and incoherently dedispersed in hardware. The sampling time was chosen to match the dispersion smearing across one filterbank channel.

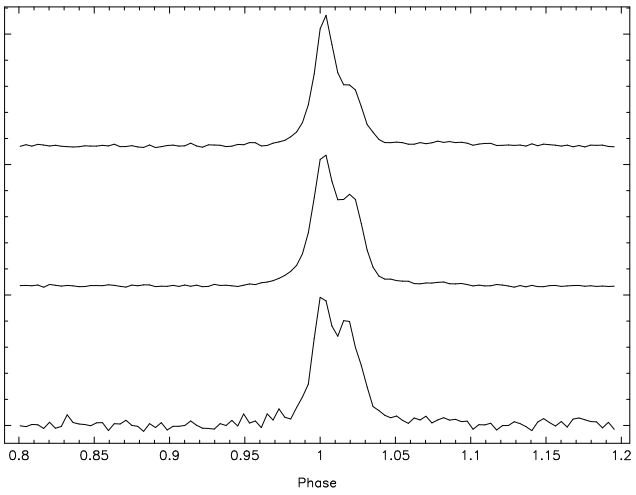

Fig. 1. Standard profiles for the three different frequencies used at Westerbork. From top to bottom: 840 MHz, 1380 MHz, 2300 MHz. The effective time resolution (102.4 μs) is similar to the size of one bin (160 μs).

At 410 MHz, a $2 \times 32 \times 0.0312$ MHz system was used, at 610 MHz we employed a $2 \times 6 \times 0.1250$ MHz filterbank, while the vast majority of our data were recorded with a $2 \times 32 \times 1$ MHz system at 1400 MHz.

The resulting dedispersed timeseries were folded on-line with the topocentric pulsar period and finally written to disc. In the off-line reduction, the two polarisations were summed to form total-intensity profiles. A standard pulse template was used at each frequency to determine the TOA. During this process, TOAs were referred to the local H-maser time-standard and already corrected to UTC using information obtained via the GPS. In our analysis, we rejected TOAs with estimated uncertainties exceeding 40 μs (or 60 μs for data prior to Jan 2000, respectively). With an average TOA error for the final data set of 18 μs, the precision of this incoherently dedispersed data set is modest, but it provides the longest time baseline in our analysis. The Jodrell Bank data were therefore used as a reference to calculate observatory-related offsets between the other data sets used.

2.3. Effelsberg

Observations in Effelsberg were made at least once a month at 1410 MHz and at irregular intervals at 850 MHz. At 1410 MHz a tunable HEMT receiver was used achieving typical system temperatures of 30-40 K depending on weather conditions and telescope elevation.

At the highest frequency a total bandwith of 55 MHz was available from the coherently dedispersing backend. For each polarisation the band was split into four subbands which themselves were subdivided into eight digitally sampled channels. Each of these 32 bands per polarisation was coherently dedispersed by programmable digital filters and then recombined with the approriate channel dispersion delay (Backer et al. 1997) and synchronously summed up with the current topocentric period.

Table 1. Individual data sets.

	Effelsberg[b]	Jodrell Bank	Nançay[b]	Westerbork	Green Bank[b]	All combined
Number of TOAs	71	292	145	126	382	1016
Time span (MJD)	52481 – 54166	49797 – 53925	53307 – 54200	51389 – 54337	49670 – 52895	49670 – 54337
R.M.S. individual data set[a] (μs)	3.3	10.7	3.3	5.2	8.2	6.0
Observed Frequencies (MHz)	1400	400, 600, 1400	1400	840, 1380, 2300	350, 370, 575, 800	

The best timing solution acquired from all data sets is presented in Table 2. (*a*) R.M.S. given require reduced $\chi^2 = 1$ for each individual data set. (*b*) R.M.S. is the result of a fit with proper motion (Green Bank, Effelsberg, Nançay) and dispersion measure (Effelsberg, Nançay) fixed.

A TOA was calculated for each average profile obtained during a 5-10 minute observation. During this process, the observed time-stamped profile was compared to a synthetic template, which was constructed out of 3 Gaussian components fitted to a high S/N standard profile (Kramer et al. 1998, 1999). This template matching was done by a least-squares fitting of the Fourier-transformed data (Taylor 1992). Using the measured time delay between the actual profile and the template, the accurate time stamp of the data provided by a local H-maser and corrected off-line to UTC using recorded information from GPS satellites, the final TOA was obtained.

Originally, multiple TOAs were calculated from one observation, but better results were acquired from calculating one TOA per observation. We have used data obtained since August 2002, having TOA errors smaller than 20 μs, on average 5μs.

2.4. Nançay

The pulsar has been observed weekly in Nançay since late 2004. Equivalent to a 93-m dish, the Nançay Radio Telescope and the BON (Berkeley-Orléans-Nançay) coherent dedispersor were used for typical integration times of 45 min. Coherent dedispersion of a 64 MHz band centred on 1398 MHz is carried out on sixteen 4 MHz channels using a PC-cluster. The Nançay data are recorded on a UTC(GPS) time scale built at the analogue to digital converter by a Thunderbolt receiver (Trimble Inc.). Differences between UTC and UTC(GPS) are less than 10 ns at maximum, and therefore no laboratory clock corrections are needed. One TOA was calculated from a cross-correlation with a pulse template for each observation of $\sim$ 45 min. Except for 24 low S/N profiles that were excluded from the used sample, all TOAs have errors less than 15 μs, but generally around 5 μs. Since the data span of Nançay Observatory covers only a few years, the proper motion of PSR J1518+4904 was fixed in determining the best timing solution for this data set alone.

2.5. Green Bank

PSR J1518+4904 was observed at Green Bank using the 140 Foot (43 m) Telescope and the 100 m Green Bank Telescope (GBT). Observations with the 140 Foot Telescope were made every few weeks from November 1994 to July 1999 at 575 and 800 MHz. Intensive campaigns, giving full coverage of the orbit over several days, were made with the 140 Foot Telescope at 370 MHz in March/April 1995, August/September 1995, May 1998, and December 1998. An intensive campaign was made using the GBT at 370 MHz in August/September 2003.

The same data acquisition system and nearly identical observational procedures were employed at the two telescopes. Details are given in Nice et al. (1996). Briefly, data were collected by the Spectral Processor, a Fourier transform spectrometer, which synthesized 512 spectral channels across a passband of 40 MHz and folded the power measurements in each channel at the topocentric pulse period to produce pulse profiles. Observation times ranged from a few minutes to several hours on any given day. During the course of an observation, data were integrated over intervals of 2 minutes (140 Foot Telescope) or 0.5 minutes (GBT). Data were separately collected in two polarizations. Off-line, each integration was processed by summing polarizations, dedispersing and summing spectral channels to produce a single pulse profile, and deriving a TOA using conventional procedures. Observations of up to one hour were averaged together by computing TOAs for individual integrations and averaging them into a single effective TOA for the hour-long span. Time stamps were provided by a local H-maser and corrected off-line to UTC using recorded information from GPS satellites. Arbitrary offsets were allowed in the timing solution between sets of TOAs collected at different frequencies, and between two sets of GBT TOAs collected with different receiver polarization settings.

2.6. Combination of data sets

Combining data sets obtained by different observatories will have many advantages. Using a longer time span sampled with more data is usually better for timing in general. The four telescopes now in use for EPTA timing purposes all contribute differently to the total picture of high-precision timing. The Westerbork, Effelsberg and Nançay data sets are of very high quality, and adding the Jodrell Bank long-term data which has only slightly lower average R.M.S. provides us with both a good coverage in time as well as in orbital phase for this pulsar. The addition of the original GBT data further complements our set of measurements of TOAs from the system.

When combining data from multiple telescopes, all with different observing and operating systems, it is important to account for all extra time corrections needed, apart from the usual correction from arrival times at individual telescopes to arrival times in TAI at the solar system barycentre[1] (SSB). Observatory-related time delays that are not accounted for (i.e. unmodelled cable delays) as well as a different approach in cal-

[1] ftp://ssd.jpl.nasa.gov/pub/eph/export/DE405/de405iom.ps

Table 2. Timing solution using data from Jodrell Bank, Westerbork, Effelsberg, Nançay and Green Bank.

Fit and data-set	
Pulsar name	J1518+4904
MJD range	49670.7—54337.7
Number of TOAs	1016
Epoch (MJD)	52000
R.M.S. timing residual (μs)	6.05
Weighted fit	Y
Reduced χ^2 value	1.117
Measured Quantities	
Right ascension, α (J2000)	$15^h18^m16\overset{s}{.}799084(16)$
Declination, δ (J2000)	$+49°04'34\overset{''}{.}25119(16)$
Pulse frequency, ν (s^{-1})	24.4289793809236(3)
First derivative of pulse frequency, $\dot{\nu}$ (s^{-2})	$-1.62263(12)\times10^{-17}$
Dispersion measure, DM ($cm^{-3}pc$)	11.61139(8)
Proper motion in RA, μ_α (mas yr^{-1})	−0.67(4)
Proper motion in DEC, μ_δ (mas yr^{-1})	−8.53(4)
Orbital period, P_b (d)	8.6340050964(11)
Epoch of periastron, T_0 (MJD)	52857.71084163(17)
Projected semi-major axis of orbit, x (lt-s)	20.0440029(4)
Longitude of periastron, ω_0 (deg)	342.554394(7)
Orbital eccentricity, e	0.24948451(3)
First derivative of orbital period, $\dot{P}_b$	$2.4(22)\times10^{-13}$
First derivative of x, $\dot{x}$	$-1.1(3)\times10^{-14}$
Periastron advance, $\dot{\omega}$ (deg yr^{-1})	0.0113725(19)
Derived Quantities	
$\log_{10}$(Characteristic age, yr)	10.38
$\log_{10}$(Surface magnetic field strength, G)	9.03
Mass function ($M_\odot$)	0.115988
Total mass, M_T ($M_\odot$)	2.7183(7)
Total proper motion, μ_T (mas yr^{-1})	8.55(4)
DM distance (pc)	625^{+90}_{-83}
Assumptions	
Clock correction procedure	TT(TAI)
Solar system ephemeris model	DE405
Binary model	DD
Model version number	5.00

Figures in parentheses are the nominal 1σ TEMPO2 uncertainties in the least-significant digits quoted. All time-dependent variables refer to the same epoch. The DM distance is estimated from the Cordes & Lazio (2002) model.

culating TOAs (template differences) will result in a time offset between sets of residuals from the different telescopes. The new timing software package TEMPO2 (Hobbs et al. 2006) is capable of fitting for constant time offsets, and these so-called "jumps", which are on the order of 0.1 ms, have been used as extra parameters in the timing model. A more detailed study on this subject will be presented in a forthcoming paper.

3. Results

The best overall timing solution for PSR J1518+4904 , obtained by combining data from Jodrell Bank, Westerbork, Effelsberg, Nançay and Green Bank, is presented in Fig. 2 and Tables 1 and 2. Before combining the data sets from the different observatories, the errors on the TOAs were scaled with a constant factor to have each individual data set return a reduced $\chi^2 \approx 1$.

Having multiple sets of TOAs allows us to select different subsets of TOAs for refining different parameters. When measuring the astrometric and rotational parameters like position, proper motion and spin frequencies, it is best to use a combination covering a data span as long as possible, in our case using all available data sets. Even though the standard deviation of the residuals from zero was, on average, somewhat larger, this yields the best possible determination of these parameters.

For short-period binaries, it can sometimes be better to select only the data set(s) with the highest precision TOAs to determine the binary parameters more accurately. We have tried several combinations of the best TOAs, i.e. using Nançay and Westerbork, or Nançay, Westerbork and Effelsberg. However, we found the best parameter measurements are derived from timing solutions which combine all data sets, not just those with the most precise TOAs. The total data set has broader orbital coverage compared to any combination of subsets having the most precise TOAs, and also covers a longer time span, improving the measurement precision of parameters that undergo secular changes. The timing parameters derived from various combinations are all in agreement with each other, showing that there are no large systematic effects in the separate data sets.

3.1. Dispersion measure variations

Although the majority of all observations were done at frequencies around 1400 MHz, Westerbork, Jodrell Bank and Green Bank have also observed PSR J1518+4904 at other frequencies, see Table 1, allowing us, in principle, to detect DM variations. We applied the "stridefit" plugin of TEMPO2 which fits small segments of time for DM while keeping all other parameters fixed. Because the observations at additional frequencies are not distributed evenly across the full time span, it was not possible to apply this method continuously. However, there is no evidence of large variations or trends present in the dispersion measure.

In a similar way as explained above, we have tried to improve our timing solution by fixing the best DM found from the solution using all available TOAs, and fitting again using only the higher precision 1400 MHz data from Jodrell Bank, Westerbork, Nançay and Effelsberg. Again, having the data set as extended as possible resulted in the better determination of the parameters.

3.2. Parallax

Even though the DM is quite small, the error in the DM-derived distance is still dominating the significance of any velocity or orientiation measurement. For a relatively nearby system like PSR J1518+4904 , it is worthwhile investigating the possibility of detecting a parallax signature in the timing residuals to be able to acquire an independent, and perhaps even better, distance estimate.

The expected amplitude in the timing residuals due to parallax (from Lorimer & Kramer 2005, §8.2.5) is $l^2 \cos\beta/2cd \sim 0.9\mu s$, where l is the distance between the Earth and the SSB, β the ecliptic latitude of the pulsar, c the speed of light and d the distance to the pulsar. Unless the TOA measurements improve significantly, we cannot expect to measure the parallax for at least another 600 years.

3.3. Proper motion

As part of the astrometric fit, we have made a significant detection of the proper motion of this system, in right ascension $\mu_\alpha = -0.67(4)$, and in declination $\mu_\delta = -8.53(4)$ mas yr^{-1}. The total proper motion is $\mu_\mathrm{T} = 8.55(7)$ mas yr^{-1} which, using the DM-derived[2] distance of 625^{+90}_{-83} pc, corresponds to a transverse velocity of just 25(4) km s^{-1}.

3.4. Shklovskii effect

The transverse motion of the system results in an increasing projected distance of the pulsar to the solar system barycentre, which affects any observed change in periodicities in the system (Shklovskii 1970).

For this pulsar, with a period of 40.93 ms, a total proper motion measured to be 8.55 mas yr^{-1} and distance estimated at 625 pc, the Shklovskii term in the period derivative will be as large as 20% of the observed $\dot{P}$. However, as will be shown in §3.6.3, this effect can be cancelled out by the acceleration towards the Galactic disc. The observed period derivative of the pulsar is therefore likely to be close to the intrinsic value. The estimate of the characteristic age τ_c and the magnetic field will not deviate significantly from the TEMPO2 calculated values as presented in Table 2.

3.5. Secular perturbation of x and $\dot{\omega}$

Because of the significant proper motion measurement, it is interesting to investigate any geometric effects that are likely to result from changes in the line of sight towards the system. For example, the varying projection of the orbit as the system moves through space can result in an apparent change in the semimajor axis of the orbit, $\dot{x}$, and a perturbation of the observed periastron advance, $\delta\dot{\omega}$. Following Kopeikin (1996), but writing in terms of position angles, these can be expressed as:

$$\dot{x} = x\,\mu_\mathrm{T} \cot i \cos(\Theta_\mu - \Omega), \quad (1)$$

$$\delta\dot{\omega} = -\mu_\mathrm{T} \csc i \sin(\Theta_\mu - \Omega), \quad (2)$$

where Θ_μ and Ω represent the direction of proper motion and the position angle of the ascending node respectively (measured North through East). When it can be shown that the proper motion is the dominant effect on the observed $\dot{x}$, Eq. 1 can be used to derive an upper limit on the orbital inclination:

$$\tan i < \mu_\mathrm{T} / \left(\frac{\dot{x}}{x}\right), \quad (3)$$

[2] The DM distance is estimated from the Cordes & Lazio (2002) model.

where we have used $|\cos(\Theta_\mu - \Omega)| \leq 1$. In this system, the effect of gravitational wave (GW) emission on the change of semi-major axis will be negligible, as it is expected to be only a fraction of the GW-effect on $\dot{P}_\mathrm{b}$, which is already undetectable (see §3.6.3), so that we can apply the above formula.

We were able to significantly measure a change in the projected semi-major axis: $\dot{x} = -1.1(3) \times 10^{-14}$. Taken at face value, our measurement corresponds to an upper limit on the inclination of 69 degrees, assuming $0° < i < 90°$. A complete analysis of the interpretation of $\dot{x}$, including all orbital orientations and including the effects of its covariance with the relativistic parameter γ, will be presented in §4.1 below.

3.6. Post-Keplerian parameters

As mentioned above, the wide orbit of PSR J1518+4904 means that it is unlikely that another PK parameter, besides $\dot{\omega}$, will be detected in the near future. However, considering that $\dot{P}_\mathrm{b}$ is the PK parameter with the strongest dependence on the total observing time span T and P_b (Damour & Taylor 1992, Table II), it will probably be measured sooner than any of the other PK parameters. Placing an exact value on the timescale it will take to measure any further PK parameters is difficult, due to the covariances with other parameters and the possibility that kinematic terms may come to dominate the timing solution. In general, measuring any further PK parameters in this system will be challenging and will require observation durations that at least double the existing observation span of 12.8 years.

We consider each of the PK parameters below. For this system we neglect any contributions to the PK parameters due to effects other than general relativity (GR) or proper motion. As spin-orbit coupling and tidal effects are only expected to be of influence for a main-sequence companion, and any significant third body in the system would have been detected in the timing residuals, we consider this a valid assumption.

3.6.1. Advance of periastron: $\dot{\omega}$

We measure a value of $\dot{\omega} = 0.0113725(19)$ deg yr^{-1} for the periastron advance of the orbit. This agrees with, and improves upon the already published values of 0.0111(2) deg yr^{-1}, 0.0113(1) deg yr^{-1} (Nice et al. 1996, 1999) and 0.01138(4) deg yr^{-1} (Hobbs et al. 2004).

Our measured $\dot{\omega}$, combined with the mass function resulting from the orbital parameters, gives a very precise total mass of the system of 2.7183(7) $M_\odot$. This value is calculated assuming GR is the correct theory of gravity and the only measurable cause of periastron advance. As can be seen from Eq.2, and shown in more detail in Fig. 7, this is likely justified, as we find the contribution to $\dot{\omega}$ from the proper motion for the possible geometric configurations of the system to be of the same order as the measurement uncertainty.

3.6.2. Shapiro delay parameters r and s

For suitable inclination angles, Shapiro delay would be readily detected in this system. However, we have not seen the signa-

ture of Shapiro delay in the data, which indicates that the orbit has a low inclination. We use this to set a limit on the inclination of the orbit by generating a map of χ^2 space resulting from fitting the mass of the companion and inclination angle in various combinations[3]. The resulting probability contours are shown in Fig. 3, along with the constraint on the total mass from our $\dot{\omega}$ measurement. In our case the contour plot results in upper limits only and there is a 99% chance that $\sin i \leq 0.73$, corresponding to an upper limit on the inclination angle of 47 degrees. Combining this limit with the $\dot{\omega}$ measurement and the mass function gives a lower limit on the companion mass of 1.29 $M_\odot$.

3.6.3. Decay of the orbit: $\dot{P}_\mathrm{b}$

Another effect of the wide orbit of the system is that the decay of the orbit due to gravitational wave damping will be very small. The relative motion effects, due to the proper motion and the acceleration in the Galactic potential, will therefore completely dominate observed changes in $\dot{P}_\mathrm{b}$ (e.g. Bell & Bailes 1996; Nice & Taylor 1995). Even with the relatively low proper motion measured for this system, the Shklovskii effect (Shklovskii 1970) on the orbit will be

$$\dot{P}_{\mathrm{b,S}} = \frac{P_\mathrm{b}}{c}\frac{v_\mathrm{t}^2}{d} = 9.5 \times 10^{-14} \quad (4)$$

where we have used the aforementioned distance of 625 pc.

The acceleration toward the disc, though of opposite sign, has roughly the same magnitude. The net bias of $\dot{P}_\mathrm{b}$ is probably in the range $\Delta\dot{P}_\mathrm{b} \sim -(1-3)\times 10^{-14}$, depending on the distance to the pulsar. The uncertainty in this bias is much larger than the expected $\dot{P}_\mathrm{b}$ due to general relativity, $\dot{P}_{\mathrm{b,GR}} \sim -1.2 \times 10^{-15}$.

Our timing solution yields an upper limit of $\dot{P}_\mathrm{b} < 2.4 \times 10^{-13}$. This is considerably larger than that expected from relativistic decay of the orbit or from kinematic effects in the Galaxy. Although $\dot{P}_\mathrm{b}$ may be the first other PK parameter to be measured as the data set is extended, the combination of the three effects prevent the use as either an independent distance estimation or the separation of the masses of the system.

4. Discussion

4.1. Masses

For any given theory of gravity, measuring PK parameters will put constraints on the masses and the inclination of the system, depending only on the individual masses and the Keplerian parameters (e.g. Stairs 2003). Figure 4 shows all the current restrictions we were able to derive from our timing solution (Table 2). The improved, highly significant $\dot{\omega}$ measurement gives us a very accurate determination of the total mass. From the non-detection of Shapiro delay parameters it is clear that the inclination of the orbit is quite low. Furthermore, the $\dot{x}$ measurement presented in §3.3, taken at face value, confirms that the system is at low inclination angles.

[3] This analysis used the TEMPO2 plugin *m2sini*. For explanation of this plugin, see Ord et al. (2006).

The relativistic time-dilation/gravitational redshift parameter, γ, is only measurable when the periastron advance is large enough to decouple its effect on the timing residuals from the measurement of the semimajor axis and its time derivative (Blandford & Teukolsky 1975; Manchester & Taylor 1977; Damour & Taylor 1992). Changing ω by only a few degrees will take several hundred years, and a detection of γ can therefore not be expected in the near future. Moreover, $\dot{x}$ turns out to be highly covariant with γ in the timing analysis. This makes an independent measurement of γ impossible and obscures the interpretation of the apparent measurement of $\dot{x}$.

To clarify the influence of all the PK perturbations on our timing data, and to calculate accurate, refined values of the stellar masses, we performed a comprehensive, self-consistent timing analysis which simultaneously incorporated all relativistic and kinematic phenomena in the timing solution.

Our primary goal was to measure or constrain the values of m_p and m_c. This procedure also finds constraints on the two angles which describe the orientation of the orbit, i and Ω. For convenience, we always represent the latter as an offset from the proper motion position angle, i.e. $\Theta_\mu - \Omega$. This angle runs between $-180°$ and $180°$, while inclination runs between $0°$ and $180°$.

The four degrees of freedom in this problem (m_p, m_c, i, and $\Theta_\mu - \Omega$) are reduced to three by noting that the two masses and the inclination are related via the Keplerian mass function equation:

$$f \equiv \frac{(m_\mathrm{c}\sin i)^3}{(M_\mathrm{T})^2} = \frac{x^3}{T_\odot}\left(\frac{2\pi}{P_\mathrm{b}}\right)^2, \quad (5)$$

where all quantities on the right side of the equation are measured to high precision. We analysed a grid of timing solutions in a three-dimensional parameter space following the approach as explained in detail in Splaver et al. (2002, 2005). For the three variables, we used M_T, $\cos i$, and $\Theta_\mu - \Omega$, and we assumed a uniform prior in each of these. For randomly oriented binary systems, $\cos i$ and $\Theta_\mu - \Omega$ each follow uniform distributions, and since $\dot{\omega}$ is well known, only a small range of M_T values need be considered, so a uniform prior is acceptable for this variable as well. For each point in our three dimensional grid, we used Eq. 5 to calculate the value of m_c and the corresponding m_p. We then used the masses and orientation angles to calculate the kinematic perturbation parameters (Eqs. 1, 2) and relativistic timing parameters according to GR (e.g. § 4.1 of Stairs (2003)).

The $\dot{\omega}$ used in the analysis was the sum of the kinematic and relativistic terms held fixed while all other pulsar timing parameters (astrometric, rotational, and Keplerian orbital parameters) were free to vary. We recorded the χ^2 of each timing solution, assigning a probability to each grid point based on the difference between its χ^2 and the global minimum. We used this ensemble of probabilities to calculate confidence regions for the parameters of interest and to place limits on the stellar masses. The results are given in Figs. 5, 6 and 7.

Figure 5 shows the orientations of the orbit allowed by the timing solution. The figure is a projection of the 95.4% confidence volume of the three dimensional analysis grid onto the

two dimensional space shown. There are four regions allowed by the timing data. The Keplerian orbital parameters, combined with the lack of Shapiro delay restrict i, but because the Shapiro delay depends on $\sin i$, the resulting constraint is degenerate: if i is allowed, so is $180^\circ - i$. Since there is a detectable $\dot{x}$, Eq. 1 restricts $\Theta_\mu - \Omega$ to two possibilities (one positive and one negative value) for any given value of i. Thus there are four regions of allowed solutions, labeled A, B, C and D in the figure.

Figure 6 shows 68.3%, 95.4%, and 99.7% confidence limits on $\cos i$ and M_T space. For reference, the figure shows lines of constant mass difference $m_\mathrm{c} - m_\mathrm{p}$, at intervals of $0.2 M_\odot$, as calculated from i and M_T, and it indicates the region at low inclination angle that is excluded because $m_\mathrm{p} > 0$ is not satisfied in that region. The confidence limits were calculated by marginalizing over the probability values for values of $\Theta_\mu - \Omega$ for a given combination of $\cos i$ and M_T.

The best-fit solutions have relatively high $m_\mathrm{c} - m_\mathrm{p}$, i.e. high companion masses and low pulsar masses, although the confidence contours stretch to much lower values of $m_\mathrm{c} - m_\mathrm{p}$. The determination of M_T is dominated by the relativistic $\dot{\omega}$, but the obtained values are perturbed by the kinematic $\delta\dot{\omega}$, given by Eq. 2. This perturbation splits the allowed values for the total mass into two regions. This can be understood by plugging the values of $\Theta_\mu - \Omega$ from each of the four regions of Fig. 5 into Eq. 2, and noting that $\csc i$ is always positive, so that $\delta\dot{\omega}$ is positive for solutions A and B and negative for solutions C and D. This means that the observed $\delta\dot{\omega}$ has been biased towards higher values for solutions A and B, so that the true relativistic $\delta\dot{\omega}$ is lower than that calculated without the kinematic correction. Since M_T is proportional to $\delta\dot{\omega}^{3/2}$, this means that the true total mass is lower for solutions A and B. Similarly, the true mass is higher for solutions C and D.

Figure 7 shows the 95.4% confidence volume projected into several two-dimensional parameter spaces. For this figure, the values of i and $\Theta_\mu - \Omega$ correspond to solution D, but the distributions of all other quantities are essentially identical for all four solution regions. We note that, for completeness, all possible values for the parameters are shown in Figs. 5, 6 and 7 however we consider it unlikely that the pulsar mass will be lower than $1 M_\odot$.

We used the probabilities from the grid analysis to constrain m_p and m_c. The results are essentially identical for all four solution regions. The central 95.4% confidence intervals are $m_\mathrm{p} = 0.72^{+0.51}_{-0.58} M_\odot$ and $m_\mathrm{c} = 2.00^{+0.58}_{-0.51} M_\odot$. If, instead of central confidence intervals, we use 95.4% confidence upper and lower limits for the individual masses, these convert to $m_\mathrm{p} < 1.17\, M_\odot$ and $m_\mathrm{c} > 1.55\, M_\odot$. Note that the apparent discrepancy between these numbers originates from different areas covered in the probability distribution. For the total mass, the 95.4% confidence intervals are $2.7188 \pm 0.0011\, M_\odot$ for solutions A and B, and $2.7217 \pm 0.0018\, M_\odot$ for solutions C and D. However, allowing any of the four solutions yields the range $2.720^{+0.003}_{-0.002} M_\odot$. This last number is the most accurate value for M_T, as it reflects the uncertainty as to which orientation of the orbit is correct.

4.2. Evolution

The system is valuable for studies of DNS evolutionary scenarios. It has been believed for a long time that supernova explosions result in high kick velocities on the remaining neutron star (Bailes 1989). Recently, it has been argued that different evolutionary scenarios can be possible in binary systems with particular mass and chemical properties (Podsiadlowski et al. 2004; Van den Heuvel 2007). The so-called electron-capture collapse of an O-Ne-Mg core of a helium star leads to a *fast* supernova explosion which is believed to be symmetric and therefore does not result in a kick of the second-born neutron star. For most DNSs in which proper motion measurements have been possible, a low space velocity has been derived. Our measurement of the proper motion of PSR J1518+4904 , implying a velocity of about 25 km s^{-1}, is consistent with the evolutionary scenario mentioned above, and another piece of evidence that not all pulsars receive a large kick at birth.

Van den Heuvel (2007) argues that the low velocity of DNS systems may be correlated with the masses of the second-formed neutron stars in DNSs being somewhat lower than normal: $1.25(6) M_\odot$. Our 95.4% limit[4] of $m_\mathrm{c} > 1.55 M_\odot$ appears to contradict this correlation.

In case of a symmetric supernova the mass lost during the explosion can be calculated by the expression $e = \Delta M_\mathrm{SN}/M_\mathrm{T}$ (Bhattacharya & van den Heuvel 1991), where e is the eccentricity and M_T the total mass after the supernova explosion. For PSR J1518+4904 this results in $\Delta M_\mathrm{SN} = 0.68 M_\odot$. If we use our 95.4% lower limit on the companion of 1.55 $M_\odot$ this leads to a core-progenitor mass of $2.23 M_\odot$, which is considered to be in the lower range for helium cores (Dewi & Pols 2003), and the progenitor star must have had a mass of about $9 M_\odot$. As these stars are believed to produce degenerate O-Ne-Mg cores (Podsiadlowski et al. 2004; Poelarends et al. 2008), this is another indication that the companion neutron star must have formed in an electron-capture core collapse. The somewhat higher companion mass can possibly be explained by assuming extra fall-back during the supernova event of $\sim 0.2 M_\odot$ (e.g. Fryer & Kalogera 2001; Fryer 2007). To allow for this amount of fallback the supernova explosion has probably been very weak. An electron-capture core collapse is the most probable explanation for the parameters of this system. However, constraining the masses even better would be very interesting.

4.3. Search for the companion

Apart from the original discovery papers Nice et al. (1996); Sayer et al. (1997), there is no report of searches for pulsations of the companion of PSR J1518+4904 . The Green Bank Northern Sky Survey, optimized to find millisecond pulsars, had a flux-density limit at 370 MHz of 8 mJy for slow pulsars (with periods above 20 ms).

The very high characteristic age and the low magnetic field imply that PSR J1518+4904 is the first-born and recycled neutron star in the system. The (unseen) second neutron star will be the young object, with a long spin period, which has proba-

[4] The 99.7% limit is $m_\mathrm{c} > 1.39 M_\odot$

bly already slowed down significantly and possibly passed the death-line to become undetectable as a radio pulsar. Moreover, if the second neutron star is still active as a radio pulsar, it has a reasonable chance of being beamed away from us. In this case, taking into account that the precession timescale of the spin axis is very long, it is not expected that the companion, if active as a pulsar, will rotate into view on a short timescale.

However to be certain that no weak pulsed signal from the second neutron star has been missed, we have searched several WSRT observations of 30 minutes at 840, 1380 and 2300 MHz for pulsations of the companion of PSR J1518+4904 . We performed an acceleration search on the data although, because of the wide orbit, the expected smearing due to the orbital motion of the companion is likely to be negligible.

In the only double pulsar system known so far, PSR J0737−3039A/B, the second pulsar is only visible for a small part of each orbit (Lyne et al. 2004). To take this possibility into account, and assuming the second pulsar would be visible in an equal fraction of the orbit as PSR J0737−3039B, we have searched another set of observations spread equally across the full orbital phase range. In all searches no evidence of pulsations of a companion were found to the limits of 1.1, 0.25 and 0.5 mJy at 840, 1380 and 2300 MHz respectively, which means that if the companion is active as a pulsar, and beamed towards us, it must be less luminous than 0.098 mJy kpc^2 at 1380 MHz.

Conclusions

Using more than 12 years of timing observations obtained by 5 telescopes, we have improved the timing solution of PSR J1518+4904 . We accurately determined the total mass of the system to be $M_{\rm T} = 2.7183(7) M_\odot$ and the proper motion $\mu_{\rm T} = 8.55(4)$ mas yr^{-1}. From our timing solution we were able to set constraints on the individual masses of the system: $m_{\rm p} = 0.72^{+0.51}_{-0.58} M_\odot$ and $m_{\rm c} = 2.00^{+0.58}_{-0.51} M_\odot$ (95.4%), and the inclination of the orbit: $i < 47$ degrees (99%).

Future prospects

As discussed above, at the present timing precision it will not be possible to detect any further PK parameters in this system on any reasonable timescale. Recently we have begun observing the system using the new PuMa II coherent dedispersion backend at the WSRT (Karuppusamy et al. 2008). These observations use a total of 160 MHz of bandwidth and thus should have at least a factor $\sqrt{2}$ improved SNR. When combined with the somewhat narrower profile obtained using coherent dedispersion (see Fig.8), this should lead to improved arrival time measurements. At present we have insufficient data to check on the long term timing precision, however the error in the individual arrival times are at least a factor two better than the previous data. These improvements might allow us to put stronger limits on the PK parameters in this system.

Acknowledgements

The Westerbork Synthesis Radio Telescope is operated by ASTRON (Netherlands Foundation for Research in Astronomy) with support from the Netherlands Foundation for Scientific Research NWO. The Nançay radio Observatory is operated by the Paris Observatory, associated to the French Centre National de la Recherche Scientifique (CNRS). The Nançay Observatory also gratefully acknowledges the financial support of the Region Centre in France. DJN is supported by NSF grant AST-0647820 to Bryn Mawr College. The 140 Foot Telescope and the Green Bank Telescope are facilities of the National Radio Astronomy Observatory, operated by Associated Universities, Inc., under a cooperative agreement with the NSF. MBP acknowledges support from the Science and Technology Facilities Council (STFC).

We would like to thank Jason Hessels for help with the search for the companion, Kosmas Lazaridis for help with Effelsberg data analysis, and Ed van den Heuvel for helpful discussions on the evolution of DNSs.

References

Backer, D. C., Dexter, M. R., Zepka, A., et al. 1997, PASP, 109, 61
Bailes, M. 1989, ApJ, 342, 917
Bell, J. F. & Bailes, M. 1996, ApJ, 456, L33
Bhattacharya, D. & van den Heuvel, E. P. J. 1991, Phys. Rep., 203, 1
Blandford, R. & Teukolsky, S. A. 1975, ApJ, 198, L27
Cordes, J. M. & Lazio, T. J. W. 2002, preprint (arXiv:astro-ph/0207156)
Corongiu, A., Kramer, M., Stappers, B. W., et al. 2007, A&A, 462, 703
Damour, T. & Taylor, J. H. 1992, Phys. Rev. D, 45, 1840
Dewi, J. D. M., Podsiadlowski, P., & Pols, O. R. 2005, MNRAS, 363, L71
Dewi, J. D. M. & Pols, O. R. 2003, MNRAS, 344, 629
Faulkner, A. J., Kramer, M., Lyne, A. G., et al. 2005, ApJ, 618, L119
Fryer, C. L. 2007, ApJ, submitted (astro-ph/0711.0551)
Fryer, C. L. & Kalogera, V. 2001, ApJ, 554, 548
Hobbs, G., Lyne, A. G., Kramer, M., Martin, C. E., & Jordan, C. 2004, MNRAS, 353, 1311
Hobbs, G. B., Edwards, R. T., & Manchester, R. N. 2006, MNRAS, 369, 655
Kalogera, V., Belczynski, K., Kim, C., O'Shaugnhessy, R., & Willems, B. 2007, Phys. Rep., 442, 75
Karuppusamy, R., Stappers, B. W., & Van Straten, W. 2008, PASP, 120, 191
Kopeikin, S. M. 1996, ApJ, 467, L93
Kramer, M., Lange, C., Lorimer, D. R., et al. 1999, ApJ, 526, 957
Kramer, M., Xilouris, K. M., Lorimer, D. R., et al. 1998, ApJ, 501, 270
Lorimer, D. R. & Kramer, M. 2005, Handbook of Pulsar Astronomy (Cambridge University Press)
Lyne, A. G., Burgay, M., Kramer, M., et al. 2004, Science, 303, 1153
Manchester, R. N. & Taylor, J. H. 1977, Pulsars (San Francisco: Freeman)
Nice, D. J., Sayer, R. W., & Taylor, J. H. 1996, ApJ, 466, L87

Nice, D. J. & Taylor, J. H. 1995, ApJ, 441, 429
Nice, D. J., Taylor, J. H., & Sayer, R. W. 1999, in Pulsar Timing, General Relativity, and the Internal Structure of Neutron Stars, ed. Z. Arzoumanian, F. van der Hooft, & E. P. J. van den Heuvel (Amsterdam: North Holland), 74
Ord, S. M., Jacoby, B. A., Hotan, A. W., & Bailes, M. 2006, MNRAS, 371, 337,342
Podsiadlowski, P., Langer, N., Poelarends, A. J. T., et al. 2004, ApJ, 612, 1044
Poelarends, A. J. T., Herwig, F., Langer, N., & Heger, A. 2008, ApJ, 675, 614
Sayer, R. W., Nice, D. J., & Taylor, J. H. 1997, ApJ, 474, 426
Shklovskii, I. S. 1970, Sov. Astron., 13, 562
Splaver, E. M., Nice, D. J., Arzoumanian, Z., et al. 2002, ApJ, 581, 509
Splaver, E. M., Nice, D. J., Stairs, I. H., Lommen, A. N., & Backer, D. C. 2005, ApJ, 620, 405
Stairs, I. H. 2003, 6, 5, Living Reviews in Relativity
Taylor, J. H. 1992, Phil. Trans. Roy. Soc. A, 341, 117
Thorsett, S. E. & Chakrabarty, D. 1999, ApJ, 512, 288
Van den Heuvel, E. P. J. 2007, AIP Conf. Proc., 924, 598
Voûte, J. L. L., Kouwenhoven, M. L. A., van Haren, P. C., et al. 2002, A&A, 385, 733

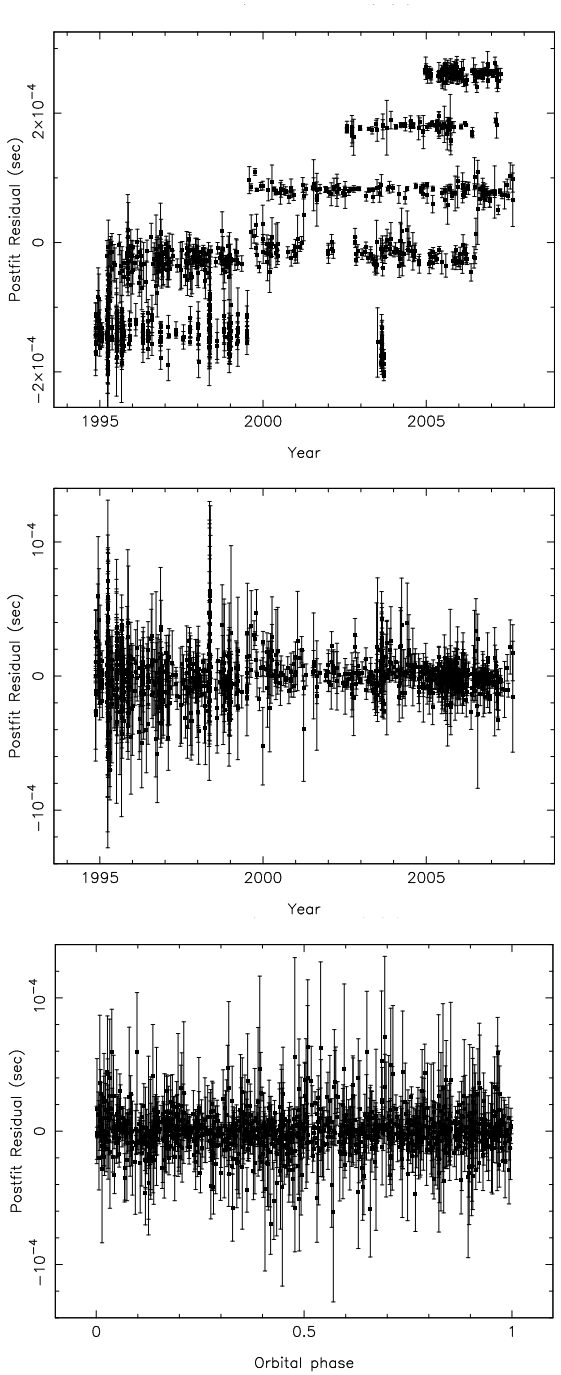

Fig. 2. Best fit timing residuals including all timing data available. The top panel shows the different data sets, from bottom to top: GBT, Jodrell Bank, Westerbork, Effelsberg and Nançay. The offsets have been adapted manually to show the data sets separately. This plot was generated from the best timing solution, which is shown in the middle panel as residuals vs time, and residuals vs orbital phase in the bottom panel. This timing solution has an rms of 6 μs and the parameters are listed in Table 2.

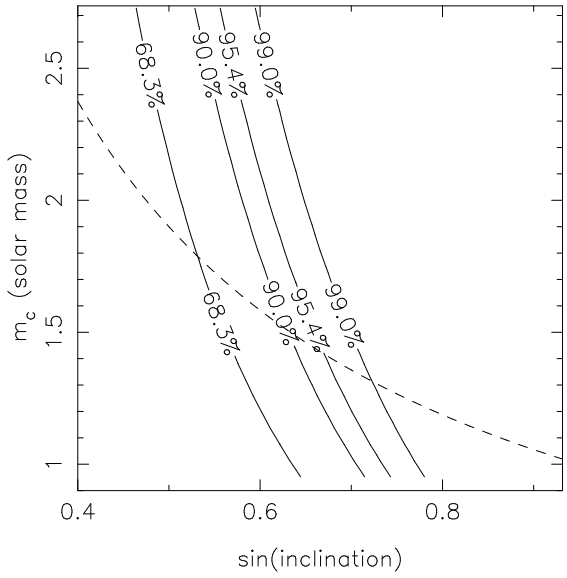

Fig. 3. Chisq contour plot of m_c-sin i parameter space. Lines with probabilities indicate regions with certain confidence levels. The dashed line represents the constraint on total mass resulting from the $\dot{\omega}$ measurement. From the non-detection of shapiro delay we can set an upper limit to the inclination of the orbit: $i < 47$ degrees. This corresponds to a lower limit for the companion mass of 1.29 $M_\odot$.

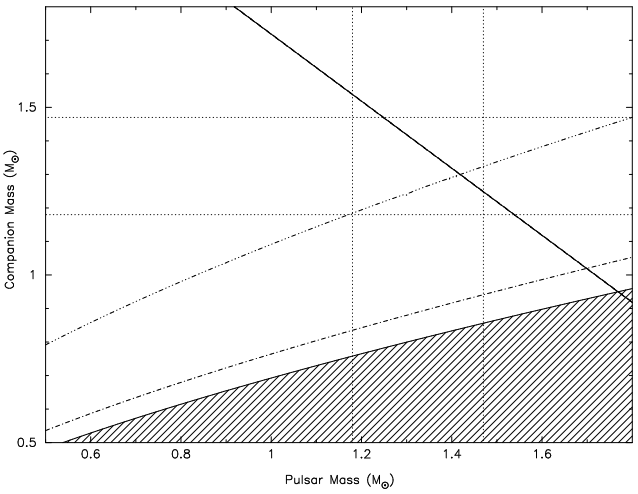

Fig. 4. Mass-mass diagram for PSR J1518+4904 and its companion. The hatched region is excluded for $i > 90$ degrees, the dash-dotted lines are indicating constraints resulting from the $\dot{x}$ measurement, $i < 69$ degrees and shapiro delay limit, $i < 47$ degrees. The diagonal line constrains $\dot{\omega}$, with errors. The dotted lines for constant pulsar and companion mass indicate the range of neutron star masses measured in other DNSs (Thorsett & Chakrabarty 1999; Lyne et al. 2004; Faulkner et al. 2005).

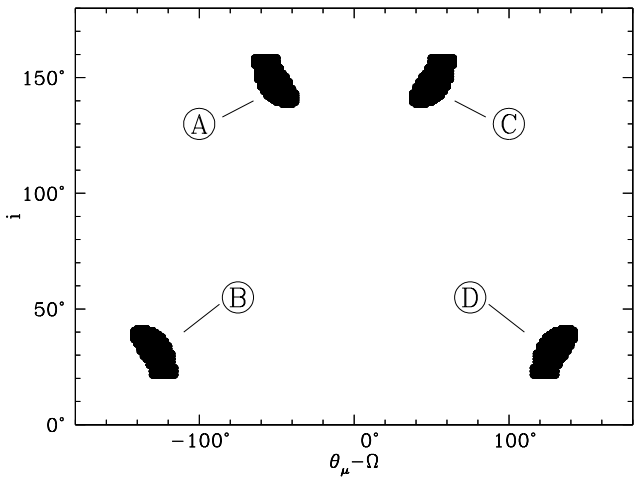

Fig. 5. Allowed values for orbital orientation i and $\theta_\mu - \Omega$. The figure shows a projection of the 95.4% confidence volume of the three dimensional grid analysis of timing solutions onto this two dimensional space. See the text for discussion.

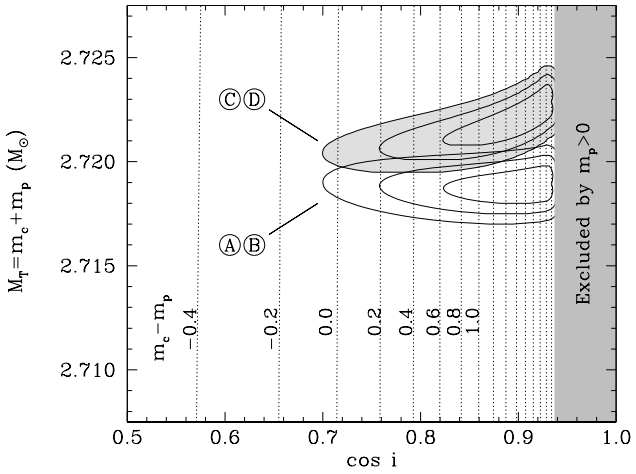

Fig. 6. Allowed values for total mass and cos i. The two sets of contours are 68.3%, 95.4%, and 99.7% confidence limits on these quantities for solutions A and B (lower, white contours) and C and D (upper, gray contours). Dotted lines indicate values of $m_c - m_p$, at intervals of $0.2 M_\odot$. The dark region on the right of the plot is excluded as it does not satisfy $m_p > 0$.

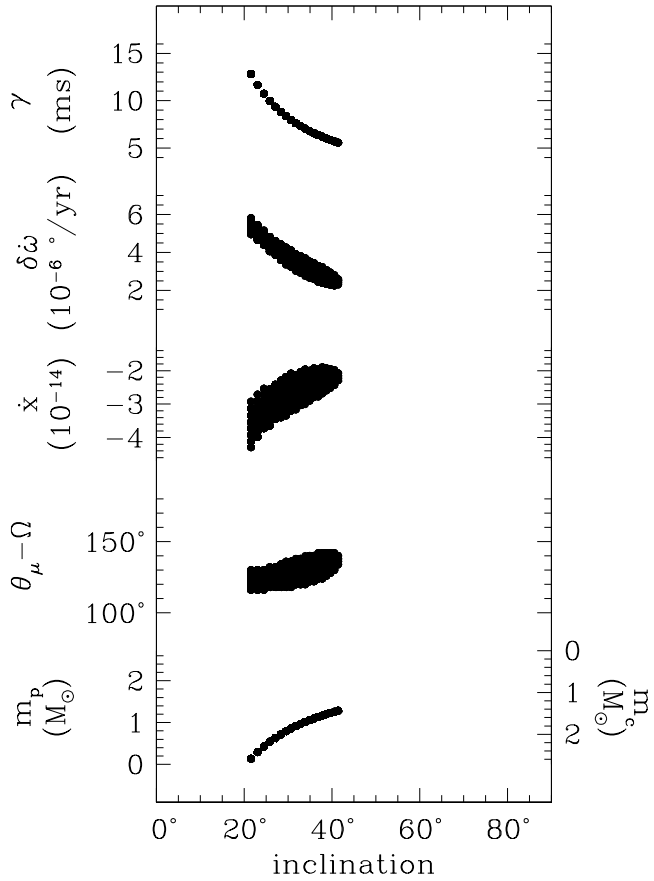

Fig. 7. Values of relativistic γ, kinematic $\delta\dot{\omega}$, kinematic $\dot{x}$, orbital orientation $\theta_\mu - \Omega$, and masses m_p and m_c allowed by the timing solution, as a function of inclination angle. The figure shows a projection of the 95.4% confidence volume of the three dimensional grid analysis of timing solutions onto each of the two dimensional spaces shown. The regions corresponds to solution *D*, but other solutions give essentially identical results.

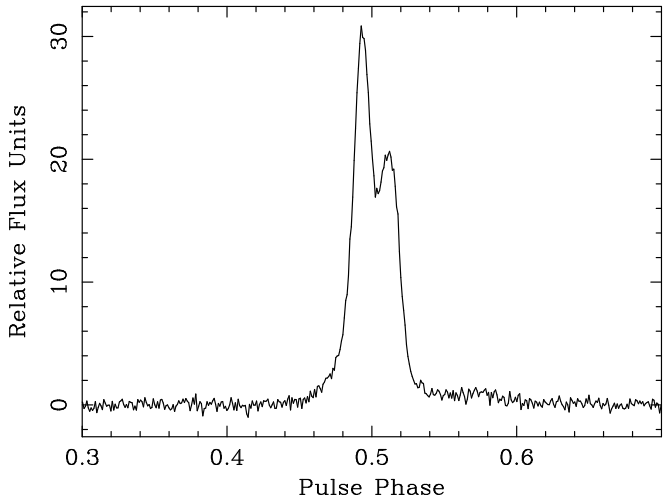

Fig. 8. A pulse profile obtained using PuMa II at the WSRT. The data were obtained in a 30 minute observation at 1380 MHz with a bandwidth of 160 MHz and were analysed using a coherent filterbank with 512 frequency channels and a time resolution of 6.4 μs. A similar pulse phase range is shown as in Fig. 1 and the improved resolution shows somewhat more detail in the pulse profile.